Title: Complexity and 1/f slope jointly reflect cortical states across different E/I balances

Authors: Medel, V[1]*., Irani, M[1]*., Ossandón, T[1,2]✉., Boncompte, G[1]✉.

[1] Neurodynamics of Cognition Laboratory, School of Medicine, Pontificia Universidad Católica de Chile, Santiago, Chile

[2] Institute of Biological and Medical Engineering, Pontificia Universidad Católica de Chile, Santiago, Chile

* Equally contributing authors

✉GB: gnboncompte@gmail.com; TO: tossandon@gmail.com

Abstract

Characterization of cortical states is essential for understanding brain functioning in the absence of external stimuli. The balance between excitation and inhibition and the number of non-redundant activity patterns, indexed by the 1/f slope and LZc respectively, distinguish cortical states. However, the relation between these two measures has not been characterized. Here we analyzed the relation between 1/f slope and LZc with two modeling approaches and in empirical human EEG and monkey ECoG data. We contrasted resting state with propofol anesthesia, which is known to modulate the excitation-inhibition balance. We found convergent results among all strategies employed, showing an inverse and not trivial monotonic relation between 1/f slope and complexity. This behavior was observed even when the signals' spectral properties were heavily manipulated, consistent at ECoG and EEG scales. Models also showed that LZc was strongly dependent on 1/f slope but independent of the signal's spectral power law's offset. Our results show that, although these measures have very distinct mathematical origins, they are closely related. We hypothesize that differentially entropic regimes could underlie the link between the excitation-inhibition balance and the vastness of repertoire of cortical systems.

Keywords: Cortical States | Lempel-Ziv Complexity | 1/f Slope | Excitation/Inhibition Balance | Anesthesia | Propofol

Introduction

Spontaneously occurring brain activity patterns in the cerebral cortex constitute the so-called cortical states (Harris & Thiele, 2011; Reimer et al., 2014). These are present without a direct link to external stimuli, and constitute the basis of essential cognitive processes like attention (McGinley(Harris & Thiele, 2011; Reimer et al., 2014) and global states of consciousness (GSC; e.g. sleep, wakefulness and anesthesia; (Bayne et al., 2016; He & Raichle, 2009). One of the most prominent strategies to characterize cortical states has been to analyze the spectral properties of their associated field potentials like electroencephalogram (EEG) and local field potential (LFP). In the particular case of attention, it has been shown that both induced (Klimesch et al., 1998) and spontaneous (Boncompte et al., 2016; Iemi et al., 2017) modulations of properties of alpha-band oscillations broadly explain the attentional state of subjects. However, the characterization of GSC in terms of the unique properties of their associated cortical states has proven to be more elusive. Traditional spectral characteristics of brain field potentials cannot fully distinguish between GSC (Purdon & Sampson, 2015). This is well illustrated for the case of anesthetics that equally produce a cease of phenomenological experiences in loss of consciousness, but show diverse spectral neural signatures. For example, transitions from wakefulness to anesthesia induced by propofol increase and frontalize alpha oscillations, while dexmedetomidine anesthesia instead induces spindle-like activity without significant modulations of alpha oscillations (Akeju et al., 2014; Huupponen et al., 2008). In recent years, new methodologies have emerged with promising results, which aim at characterizing background cortical states in general, but also specifically for GSC.

Cortical neurons in awake animals show strong membrane potential fluctuations which cause irregular discharge similar to a Poisson process, known as high conductance states (Destexhe et al., 2003). These states generate the background activity that support high-order processes are computed. It has been shown that neurons can achieve irregular firing patterns with balanced excitatory and inhibitory synaptic activity (van Vreeswijk & Sompolinsky, 1996; Brunel, 2000). From this perspective, cortical states depend on global brain variables, such as relative levels of excitation and inhibition (Haider et al., 2006). Moreover, from local circuit activity to whole-brain modeling, the computational characterization of the balance between excitation and inhibition (E/I balance) has shown to modulate information transmission and entropy (Deco et al., 2014; Rubin et al., 2017; Agrawal et al., 2018). On the other hand, perturbations in the E/I balance has shown to be related with pathological brain activity (Žiburkus et al., 2013) and neuropsychiatric disorders (Haider et al., 2006; Uhlhaas & Singer, 2010; Rubenstein & Merzenich, 2003; Sohal & Rubenstein, 2019). A particularly successful way to quantify E/I balance is the slope of the power law decay of spectral power of brain field potentials. Specifically, models have been shown that the background 1/f slope of the power spectral density (PSD) emerges from the sum of stochastic excitatory and inhibitory currents (Destexhe et al., 2001; Sheehan et al., 2018; Gao et al., 2017). Moreover, empirical validation of these models has shown that the E/I balance can be properly inferred from background activity by parameterizing the 1/f shape of the PSD (Gao et al., 2017; Trakoshis et al., 2020).

Interest in the detailed informational structure of cortical states has produced a recent surge of information-theory based approaches (Arsiwalla & Verschure, 2018; Ferenets et al., 2006; Sarasso et al., 2014; Zhang et al., 2001). Data analysis strategies based on Lempel-Ziv complexity (LZc; Lempel & Ziv, 1976), like the Perturbational Complexity Index (Casali et al., 2013) have been successful for characterizing subject's GSC during dreamless sleep and during anesthesia-induced unconsciousness, with independence of the anesthetic used. It has been shown that LZc decreases concomitantly with the loss of phenomenological possibilities, which is consistent with theoretical views of consciousness (Tononi & Edelman, 1998). Lempel-Ziv complexity algorithm computes the number of non-redundant segments of a signal (Lempel & Ziv, 1976), which in turn, when applied to brain data, is related to the abundance of the repertoire of brain activity patterns observed (Wenzel et al., 2019). During the transition from wakefulness to sleep or anesthesia, the number of possible experiences and cognitive processes that one can have is greatly reduced. Thus, it is expectable that the complexity of brain activity follows the same pattern. In fact, this reduction of the repertoire of brain activity has been seen in rats at the single neuron level using a myriad of convergent measures of cortical diversity, including LZc (Wenzel et al., 2019) which suggests that LZc can be applied as a multiscale proxy of neural repertoire.

Although 1/f slope and LZc have distant mathematical origins, one coming from spectral analysis and the other from Information Theory, both have been shown to correlate with GSC (Miskovic et al., 2019; Zhang et al., 2001). We hypothesize that this could be due to an underlying intrinsic relation between E/I balance and the repertoire of activity patterns in cortical systems. Here we employed three complementary approaches to study the possible relation between 1/f slope and LZc and thus implicitly between E/I balance and the abundance of non-redundant repertoire in brain field potentials. We analyzed this relation in: (i) a simple inverse Discrete Fourier Transform (iDFT) model, (ii) a cortical field potential model, (iii) human EEG data, and (iv) monkey ECoG anesthesia data. Our results consistently show a non-trivial relation between 1/f slope and LZc in brain field potentials, and suggest that both could be related to the underlying entropy rate of the system..

Materials and Methods

iDFT Models

To study the relation between the power-law slope of neuronal signals and their complexity in time, we first employed an iDFT modeling strategy. We constructed signals with different 1/f slopes, among other spectral parameters, and analyzed their resulting LZc. Each signal was simulated using 5 seconds of length sampled at 1KHz, which resulted in a Nyquist frequency (N_f) of 500Hz. Each time series was initially constructed in the frequency domain as the product of its amplitude and phase components. The amplitude of each frequency component was set accordingly to a power-law distribution, as illustrated in Equation 1:

$$A(f) = O * f^{-s} \qquad (1)$$

where *f* is the frequency of each term, *A(f)* is the amplitude of each frequency component, *O* is the offset of the curve, the amplitude of the 1 Hz component, and *s* corresponds to the slope of the power-law. Each initial phase was randomly assigned from a uniform distribution ($-\pi$ to π). iDFT algorithm (as implemented in Numpy; (Virtanen et al., 2020) was applied to the product of the amplitude (*A(f)* and phase components to obtain the time series data according to Equation 2:

$$signal(t) = iDFT\,(A(f) * exp(i * \theta_0) \qquad (2)$$

where *i* is the imaginary unit, and θ_0 corresponds to the initial phase of each frequency. Only positive frequencies were employed. To better model the spectral properties of physiologically plausible neural signals, in addition to constructing signals using the whole range of possible frequencies (0 to N_f) we also applied two types of constraints to the power-law distribution: an initial frequency (f_0) and a final frequency (f_f). Both of these are illustrated in Figure 1A. Specifically, f_0 corresponds to setting all amplitudes of frequencies lower than f_0 to the value of f_0, thus flattening the curve to the left of f_0. On the other hand, applying a f_f corresponds to setting the amplitude of every frequency higher than f_f to zero. To maintain time series stationarity, a requirement of the LZc algorithm (Lempel & Ziv, 1976; Zhang et al., 2001), all iDFT models were made with a f_0 = 1Hz unless otherwise stated. For every set of simulations, we generated a 256 time series with different values of *s*.

LZc algorithm

To compute the complexity of time series (both simulated and empirical), we used the Lempel-Ziv Complexity algorithm as introduced by Lempel and Ziv (Lempel & Ziv, 1976). This algorithm quantifies the number of distinct and non-redundant patterns of a signal and it can serve as a close analogue of the entropy rate of a signal (Amigó et al., 2004). We implemented the LZ76 algorithm using custom made Python scripts (available in Supplementary Materials). Briefly, every time series was first binarized, assigning a value of 1 for each time point with an amplitude greater than the median of the entire signal (5 s), and zero for those below it. Afterwards, the LZ76 algorithm was applied to the resulting so-called symbolic signal. To quantify the number of non-redundant patterns, a sequential

evaluation of the signal is performed. At each point, the algorithm analyzes whether the following segment of the signal can be recreated from the already analyzed signal. In this sense, if the following sequence is not contained in the previously analyzed signal, then the complexity increases. If the next sequence is already contained in the already analyzed signal, the algorithm advances without increasing the complexity. An illustrative description of the algorithm for two sample sequences can be found in supplementary materials (Supplementary Figure 1). The number of non-redundant patterns in a signal is then normalized to produce the final LZc value, which ranges (asymptotically for long signals) from 0 to 1. The LZ76 algorithm has been widely applied to analyze neural signals, from spike trains to EEG field potentials;, however, it should not be mistaken with the similar Lempel-Ziv-Welch algorithm (Welch, 1984), also recently employed in neurocognitive studies (Schartner et al., 2015). Although these two share commonalities, to our knowledge the link between complexity and entropy rate has only been established for the LZ76 algorithm.

1/f slope vs. LZc modeling function

We found that the relation between 1/f slope and LZc in pure power-law iDFT data (Figure 1B) closely followed a particular mathematical behavior:

$$LZc(s) = a_1 * exp\,(-b\ *\ ln^2(s^c\ + 1)) \quad (3.1)$$

where s is the slope of the power-law, $LZc(s)$ is the LZc value obtained for a signal with slope s and a_1, b and c are free parameters such that a_1 ranges from 0 to 1 and b and $c \in \mathbb{R}^+$. The parameters b and c modify the shape of the curve, while a is a scaling factor. Without this scaling factor, the image of $LZc(s)$ ranges from (0 to 1), while if a_1 is introduced it ranges from (0 to a_1) without changing the internal structure of the curve. While Equation 3.1 appropriately adjusted to pure power-law signals (Figure 1B) and iDFT-data generated with a non-trivial final frequency ($f_f \neq N_q$; Figure 1D), the LZc values for signals with non-trivial f_0 (> 1Hz) did not ranged from 0 to 1 but from a value greater than zero to 1 (Figure 1C). Because of this, we designed a similar equation that better reflected the required image of the $LZc(s)$ function for non-trivial f_0 cases, introducing a second scaling parameter a_2:

$$LZc(s) = a_2 + (1 - a_2) * exp\,(-b\ *\ ln^2(s^c\ + 1) \quad (3.2)$$

For every fit we employed Equations 3.1 or 3.2 using an algorithm that minimized the squares of the differences between data and models as implemented in the *scipy.optimize.curve_fit* function (Virtanen et al., 2020). Best fit parameters and R^2 values for goodness of fit for all iDFT simulations can be found in Supplementary Table 1 (all $R^2 > 0.98$).

LFP Simulations

To simulate cortical LFP time series, we employed the strategy recently developed by Gao et. al. (2017) where LFP time series are constructed based on modeled inhibitory and excitatory

conductances. Briefly, inter spike intervals were generated by Poisson processes (Destexhe et al., 2001) with specified average firing rates for GABA-A (inhibitory) and AMPA (excitatory) neurons. This produced binary time series describing firing at each time point. These spike time series were then convoluted with empirically defined conductance kernels for excitatory and inhibitory synapses independently (Alain Destexhe et al., 2003; Gao et al., 2017). Each kernel was constructed as the sum of an exponential growth and an exponential decay function, which were specific for excitatory and inhibitory synapses (CNRGlab; http://compneuro.uwaterloo.ca/research/constants-constraints/). Current time series were then obtained by multiplying each conductance by the difference between the resting potential and the typical reversal potential of AMPA and GABA-A receptors. Finally, the LFP time series were computed as the sum of excitatory and inhibitory currents (Mazzoni et al., 2015). The particular parameters used in LFP simulations can be found in supplementary material (Table S2), which are based on previous electrophysiological results and modeling of LFP (Gao et al., 2017).

For each particular simulation, we manipulated firing rate and EI-balance. Each firing rate was defined as a parameter to generate inter spike intervals following a Poisson process. EI-balance, defined as the ratio between mean excitation and mean inhibition conductances, was manipulated by a multiplicative parameter applied only to inhibitory conductances (Gao et al., 2017), such that mean inhibition current was 2 to 10 times greater than the mean magnitude of excitation conductances. Each simulated LFP time series consisted of 5s, and was downsampled to 1KHz to match iDFT simulations. We employed this modeling strategy because it has been shown to capture amplitude and spectral characteristics of synaptic conductances observed in vivo (Destexhe et al., 2001), and has been previously validated as a tool to infer the E/I balance of cortical tissues (Gao et al., 2017).

Power Spectral Density and 1/f analysis

We employed the same approach to estimate the power-law slope of LFP simulations, human EEG and monkey ECoG data. This consisted of calculating the Power Spectral Density (PSD) by means of Fourier Transforms using Welch's method as implemented in the MNE toolbox (Gramfort et al., 2014; Jas et al., 2018). Afterwards, the power-law 1/f slope and offset were obtained using the “Fitting Oscillations & One Over f” (FOOOF) toolbox (Haller et al., n.d.). Aperiodic offset (*O*) and slope (*s*) components are obtained by modeling the aperiodic signal according to Equation 1. The FOOOF algorithm decomposes the log power spectra into a summation of narrowband Gaussian periodic (oscillations) and the aperiodic (offset and slope) components for the whole frequency range. The algorithm estimates periodic and aperiodic components, removes the periodic ones and estimates again until only the aperiodic components of the signal remain. This allows for estimation of offset and power-law slope with considerable independence from oscillatory behavior, which is particularly important for empirical signal analysis (Haller et al., n.d.; Voytek & Knight, 2015). FOOOF toolbox also contains a “knee” parameter, which was not considered as it corresponds to changes in the 1/f slope at higher frequencies, not analyzed in this study. With this we obtained the 1/f slope and offset

estimates of each time series. For our analyses we performed the FOOOF fitting using a frequency range from 1 to 70 Hz for simulated and ECoG data, and 1 to 40 Hz in EEG data.

ECoG Data

We used an open ECoG database collected from 2 macaque monkeys (Chibi and George) during wakefulness, propofol anesthesia (5 and 5.2 mg/kg), and recovery (Yanagawa et al., 2013z). Propofol induced anesthesia was achieved through intravenous propofol injection. Loss of consciousness was defined as the moment when monkeys no longer responded to touch stimuli. The ECoG grid consisted of 128 channels using multichannel ECoG electrode arrays (Unique Medical, Japan). The array was implanted in the subdural space with an interelectrode distance of 5 mm. Electrodes were implanted in the left hemisphere continuously covering frontal, parietal, temporal and occipital lobes. No further preprocessing than the one used by (Yanagawa et al., 2013) was applied to this data. Since we were interested in assessing differences between brain states during wakefulness and anesthesia and not in the transitions, we only considered periods of closed-eyes wakefulness and anesthesia. We computed LZc and 1/f slope measures of the times series as mentioned above for each electrode, epoch and subject and then averaged LZc and 1/f slope across epochs. These results are shown in Figure 3.

EEG Data

We analyzed an open human propofol anesthesia EEG database (Chennu et al., 2016). We only analyzed data collected during baseline and moderate sedation conditions. In each state, subjects performed an auditory discrimination task. After the task, during closed eyes resting state, EEG data was recorded with high-density 128 electrodes caps and the Net Amps 300 amplifier (Electrical Geodesic Inc., Eugene, Oregon, USA) for ~7 minutes. Only channels covering the scalp area were retained, which resulted in 91 channels for further analysis. Moderate sedation was induced by target-controlled infusion of propofol, with targeted plasmatic propofol levels of 1.2 mcg/ml. Because the level of propofol sedation is near the anesthetic threshold of unconsciousness, and not sufficient for deep anesthesia, we collected data from the two subjects who lost the most performance. This was assessed by the number of correct responses in the auditory discrimination task during moderate sedation compared to the baseline condition. EEG signals were filtered between 0.5 Hz and 45 Hz and segmented into 10-second epochs (ranging from 37 to 40 epochs per subject). Data was re-referenced to the average of all channels. We did not apply any further preprocessing steps besides those described by Chennu et al. (2016) for the analysis presented here. Further details of procedures regarding data collection and preprocessing can be consulted in the original paper. Finally, for each epoch (time segment) and electrode, we calculated LZc and 1/f slope and then averaged across epochs.

Statistical analysis

Experimental data was visualized using raincloud plots (Allen et al., 2019; van Langen, 2020). Statistical significance was assessed with a Type-1 error threshold of 0.05. All curve fits were carried

out using Scipy optimize function. R^2 were calculated using custom made scripts. Differences among groups in 1/f slope (Figure 3A, B) and LZc (Figure 3C, D) were assessed by two-way ANOVAs for each measure. Conscious state (awake vs. anesthesia) and the subject's identity were used as ways. We included both humans and monkey datasets in these ANOVAs. Afterwards, simple main effects for conscious states were performed for each dataset, comparing awake vs. anesthesia for each human and monkey individually. To estimate the relation between 1/f slope and LZc in ECoG and EEG data, for each subject and electrode, we adjusted a linear curve to 1/f slope and LZc data across epochs (time segments). The Pearson product-moment correlation coefficient for each one of these fits was used as the dependent variable in a two-way ANOVA analysis (Figure 3E, F). Simple main effects were applied in the same way as for the analysis of each individual measure.

Results

iDFT Model

In order to analyze the relation between the spectral power-law slope and the LZc, we generated, by means of iDFT, sets of 256 time series with different slopes (e.g. blue trace in Figure 1A) ranging from 0 to 2, and calculated the complexity values for each one. We found that, for pure power-law time series, the relation between slope and LZc follows a strict monotonically descending behavior (Figure 1B), with lesser complexity values for time series with a steeper slope. This general behavior is expected: slopes near zero reflect white noise (maximal LZc), while on the other hand, very high slopes reflect time series with significant power only in low frequencies (periodic signals with minimal LZc). Interestingly, we found that LZc had a one-to-one mapping with 1/f slope. This relation can be robustly adjusted (R^2 > 0.99) to an x-inverted asymmetrical sigmoid function (see Methods, Equation 3.1).

Electrophysiological field potential signals (e.g. EEG and ECoG) have been shown to present only partial power-law behavior (He, 2014). In other words, only part of their spectrum follows a clear spectral power law distribution. In an attempt to broadly emulate this, we introduced two types of constraints to the spectra of signals: an initial (f_0) and a final (f_f) 1/f frequency (see Methods). Both constraints are illustrated in Figure 1A (orange trace for f_0; green trace for f_f). We found that the introduction of greater f_0 values (Figure 1C) generated signals with greater complexity across all slopes tested. This effect was enhanced for higher slopes compared to lower slopes (Figure 1C). Interestingly, the introduction f_0 higher than 1Hz reduced the dynamical range of the observed LZc (no longer ranging from 0 to 1). On the other hand, when we included a final frequency f_f to the generated signals (a type of low-pass filter), we also found LZc values were reduced, in comparison to the pure power law signals. This effect was more markedly observed in signals with lower slope values. Similarly to f_0, we found that f_f reduced the dynamical range of possible complexity values, but in a different way: LZc ranged from zero to a value lower than 1. Regardless of these spectral constraints, we found that the slope vs. LZc behavior could be modeled with a simple set of related equations (Equations 3.1 and 3.2), with a robust goodness of fit (all R^2 > 0.98, see Supplementary Materials).

LFP model

Spectral 1/f power law slope has been suggested as a proxy for the background state (Destexhe et al., 2001) and the balance between excitation and inhibition in cortical circuits (Destexhe et al., 2001; Lombardi et al., 2017; Gao et al., 2017; Trakoshis et al., 2020). In this line, we hypothesized that E/I balance could also be related to the repertoire of cortical activity as indexed by LZc. To test this hypothesis in a more physiologically plausible model, we simulated LFP signals as a linear combination of excitatory and inhibitory currents (see Methods; Destexhe et al., 2001). We conducted simulations with different global firing rates and E/I ratios by parameterizing inhibitory conductances (Fig 2A; see Methods). For each simulated time series, we calculated LZc and the spectral parameters of 1/f slope and offset using the FOOOF toolbox (Haller et al., n.d.).

Consistent with previous findings using this model (Gao et al., 2017), we found that manipulating E/I balance consistently modulated the offset of the 1/f behavior. However, offset was also strongly modulated by global cortical excitability (firing rate; Figure 2B). We found that the 1/f slope was also robustly modulated by E/I balance; however, in contrast to offset, the slope was completely independent of global excitability (Figure 2C). Interestingly, we found that LZc strongly correlated with E/I balance, with more excitation leading to a smaller repertoire of cortical activity patterns, and a more balanced neural population activity presenting higher complexity (Figure 2D). Similar to 1/f slope, we found that the effect of changing E/I balance on LZc was independent of the global firing rates of the simulated neural time series.

Given that E/I balance robustly modulated both 1/f slope and LZc, with independence of the firing rate, we next asked whether the relation observed between 1/f slope and LZc seen in our iDFT model could be reproduced in this more plausible cortical model, and if E/I balance tracked this relation. Figure 2E depicts the average LZc and 1/f slope for 100 simulations with their corresponding E/I balance values. It illustrates that there is a non-trivial inverse relation between these two measures, as for the iDFT model. As expected, we found that higher E/I balance was associated with flatter slopes and with higher complexity values, while when E/I balance was dominated by inhibition, complexity was reduced and PSD showed steeper slopes. Interestingly, we also found that this behavior could be well adjusted to Equation 3.1. We believe this result proposes a plausible biological mechanism of the observed relation between LZc and the power-law exponent.

Experimental Data

Next, we asked whether the impact of modifying E/I balance on the relationship between 1/f slope and LZc seen in our model could be reproduced in electrophysiological data. We first analyzed two high-density datasets, human EEG and macaque monkey ECoG recordings under propofol anesthesia and eyes-closed resting-state (Chennu et al., 2016; Yanagawa et al., 2013). Propofol is known to directly enhance GABAergic inhibitory activity, and thus reduce E/I balance (Alkire et al., 2008). In accordance with our previous results, we observed markedly increased 1/f slope (conscious state main effect's $F(1) = 1034$, $p < 0.001$, $\eta^2 = 0.467$; simple main effects (awake vs. anesthesia) for all humans and monkeys showed significant differences, $p < 0.001$) and reduced LZc with respect to wakefulness in both monkeys and in one human (conscious state main effect $F(1) = 442$, $p < 0.001$, $\eta^2 = 0.063$; simple main effects (awake vs. anesthesia) for subjects except one human showed significant differences, $p < 0.001$, Supplementary Figure 2). This is illustrated for representative EEG and ECoG datasets in Figure 3 A-D).

In addition to the individual changes observed to LZc and 1/f slope due to anesthesia, we analyzed the specific relation between these two measures and how it changed due to an increase in inhibitory activity. To this end, we analyzed the correlation, across electrodes, between 1/f slope and LZc. We found a significant and marked inverse relation in both datasets, in accordance with the results of both our models. The correlation between these two measures was consistently found for all datasets

354 analyzed (all $p < 0.05$; see also Supplementary Materials). Interestingly, this correlation was strongly
355 modulated by the propofol-induced reduction in E/I balance. In EEG data we observed an increase in
356 the Pearson product-moment correlation coefficient between 1/f slope and LZc (all simple main effects
357 $p < 0.001$). In contrast, ECoG data showed a reduction of this coefficient in response to propofol (all
358 simple main effects $p < 0.001$). We believe this apparent discrepancy (increase in EEG and decrease
359 in ECoG), is due to different baseline levels of LZc and 1/f slope across species (see Discussion).
360
361

Discussion

In this article we explored the possible relation between two apparently dissimilar time series characteristics of brain field potentials. Our results show a robust and inverse relation between LZc and 1/f slope, constitutive of a one-to-one mapping in both synthetic and experimental data. This relation closely followed an x-inverted asymmetric sigmoid function in the whole range of both measures in synthetic data generated by iDFT models. This behavior was, although scaled, present even when the spectral power law behavior only comprised a small portion of all frequencies of the signal (Figure 1C, D). This is of particular importance as real electrophysiological signals do not show a 1/f spectral power decay in the whole frequency range (He et al., 2010). In a more neurobiologically plausible model, we observed a similar inverse relation between LZc and 1/f slope, which adjusted to the same mathematical function. Moreover, we show that this relation follows the balance between excitation and inhibition, with greater complexity and flatter 1/f slopes associated with the predominance of excitatory over inhibitory activity. At the same time, although the offset was modulated by E/I balance, the complexity of the signal was completely independent of the offset. We probed this link between E/I balance and LZc by directly contrasting 1/f slope and LZc changes due to a pharmacological intervention. Propofol, a GABA agonist, produced changes in both measures consistent with what our models predicted: a reduced LZc and increased 1/f slope in both human EEG and monkey ECoG data.

The slope of the spectral power law has been linked to E/I balance (Lombardi et al., 2017), while LZc reflects the vastness of the repertoire of brain activity patterns (Wenzel et al., 2019). Although these two measures may seem unrelated at first, we hypothesize that both reflect a specific type of entropy of cortical systems. The entropy of a system can be characterized by the probabilities of each of its possible states (Shannon entropy), but also in terms of the probabilities of the transitions between these states in time, namely its entropy rate (or transition entropy). Low values of 1/f slope represent a flatter power spectrum, which is characteristic of irregular desynchronized cortical states, while steeper 1/f slopes showcase mainly low frequency periodic behavior (Fazlali et al., 2016; Voytek & Knight, 2015). These two extremes can also be characterized in terms of their signals' transition entropy: flat 1/f slopes (similar to white noise) have low autocorrelations and thus high entropy rates, while in mainly periodic signals, its history strongly constrains future values; thus they present low transition entropies. Interestingly, Amigó et al. (2004) have shown for electrophysiological signals that LZc closely reflects the entropy rate of the underlying system. This is particularly useful as direct estimations of entropy rate require much longer data series than LZ76 (Amigó et al., 2004). In our implementation of LZc, because we binarize each signal based on its median value, the number of points in each state (ones and zeros) is equal, which results in a constant Shannon or distribution entropy. In this line, we believe signal’s LZc could be reflecting not only the vastness of the repertoire of cortical activity, but also specifically the transition entropy of the system. Thus, the strong relation we observe between LZc and 1/f slope suggests both measures are, at least partially, driven by the transition entropy of the underlying cortical system.

In addition to the 1/f slope, the PSD offset has been shown to reflect relevant physiological information (Miller et al., 2014; Manning et al., 2009). Changes in the offset have been suggested to be linked to the fMRI BOLD signal, making it a potential bridge between different spatial and temporal scales of brain features (Wen & Liu, 2016). Moreover, computational modeling has shown that broadband spectral shifts reflect changes in local neural populations' total firing rate (Miller et al., 2009; Wen & Liu, 2016). Our results show that quantifying aperiodic activity while manipulating the E/I balance and firing rates reveals that only the offset is specifically modulated by firing rate (Figure 2B) while the slope was only specifically modulated by shifts in E/I the balance (Fig. 2C). In addition, LZc was not dependent on the firing rate, but was strongly regulated by E/I balance. Although we observe a relation between 1/f offset and LZc, this effect is not specific as the same offset can result from many E/I balances and firing rates combinations (Figure 2B, Supplementary Figure 2). Previous spike model simulations have shown that E/I balance is strongly related to the entropy of the modeled system (Agrawal et al., 2018). In this line, we believe the relation found here between 1/f and LZc suggests that the transition entropy and the E/I balance of cortical systems could be more closely linked than previously thought.

Future work should include the role of oscillations, as recent evidence has suggested that low frequency 1/f slope is dependent on alpha-band activity (Becker et al., 2018). Despite this potential limitation of our simulations, which lacked oscillations, we observe the same general behavior in EEG and ECoG data, which does present oscillatory activity. It should be noted that the exponent of the power-law has been characterized in different frequency ranges across the literature (He et al., 2010; Becker et al., 2018; Lombardi et al., 2017; Miskovic et al., 2019; Trakoshis et al., 2020; Schaworonkow & Voytek, n.d.). In this line, the frequency ranges that we employed here were based on generating interpretations that could be extrapolated for both local and global measures of field potentials. Moreover, we have shown that changing the initial and cut-off frequency of the power-law decay does not qualitatively affect the relation between 1/f slope and LZc (Fig. 1C, 1D). From this perspective, our results suggest that 1-70 Hz and 1-40 Hz frequency ranges share the characteristic of representing the global state of cortical activity. Further work could include the modeling of tight and loose coupling regimes between excitation and inhibition, which has been suggested as a more plausible mechanism of cortical E/I balance regulation (Dehghani et al., 2016; Denève & Machens, 2016; Trakoshis et al., 2020; Denève & Machens, 2016). These limitations are probably why we also observe a reduced range of both LZc and 1/f slope, despite modeling a broad E/I balance range. We observe a consistent relation between 1/f slope and LZc across two models and two brain field potential datasets despite this limitation.

The E/I-balance shapes cortical neurons' computational properties (Denève & Machens, 2016), and therefore behavior and cognition (Harris & Thiele, 2011). Alterations of this balance have been related to schizophrenia (Uhlhaas & Singer, 2010), autism (Rubenstein & Merzenich, 2003), and epilepsy (Žiburkus et al., 2013), which suggests it might also play an unexplored role in other neuropsychiatric disorders (Sohal & Rubenstein, 2019). Moreover, E/I balance is not a static property of the cortex. It

changes depending on the behavioral state (Waschke et al., 2019), task demands (Pfeffer et al., 2018; Waschke et al., 2019), performance (Sheehan et al., 2018) and depending on circadian rhythms (Bridi et al., 2020), which suggests that this property is under fine dynamic control. It has been proposed that cortical states and neural complexity could be regulated by subcortical cholinergic and noradrenergic activity (D'Andola et al., 2018); (Nghiem et al., 2020). Future research could address this topic with a multiscale approach to the underlying cortical states of neuromodulation-related psychiatric disorders (Medel et al., 2019). From this perspective, the readout of E/I balance through brain signal complexity and the power-law of the PSD could be useful for addressing fundamental questions about the modulation of the state dependence of cortical computations. This offers new methods to understand the general mechanisms of cortical states functioning, as well as broadening the diagnostic and therapeutic tools related to neuropsychiatric disorders.

Acknowledgments

We would like to thank Chile's national agency for science ANID for their financial support to GB (postdoctoral project N° 3200248), TO (FONDECYT N° 1180932) and to VM (doctoral scholarship N° (21180871). We also thank Fernanda Weinstein for her valuable comments on previous versions of this manuscript.

References

Agrawal, V., Cowley, A. B., Alfaori, Q., Larremore, D. B., Restrepo, J. G., & Shew, W. L. (2018). Robust entropy requires strong and balanced excitatory and inhibitory synapses. *Chaos* , *28*(10), 103115.

Akeju, O., Pavone, K. J., Westover, M. B., Vazquez, R., Prerau, M. J., Harrell, P. G., Hartnack, K. E., Rhee, J., Sampson, A. L., Habeeb, K., Gao, L., Pierce, E. T., Walsh, J. L., Brown, E. N., & Purdon, P. L. (2014). A comparison of propofol- and dexmedetomidine-induced electroencephalogram dynamics using spectral and coherence analysis. *Anesthesiology*, *121*(5), 978–989.

Alkire, M. T., Hudetz, A. G., & Tononi, G. (2008). Consciousness and anesthesia. *Science*, *322*(5903), 876–880.

Allen, M., Poggiali, D., Whitaker, K., Marshall, T. R., & Kievit, R. A. (2019). Raincloud plots: a multi-platform tool for robust data visualization. *Welcome Open Research*, *4*, 63.

Amigó, J. M., Szczepański, J., Wajnryb, E., & Sanchez-Vives, M. V. (2004). Estimating the entropy rate of spike trains via Lempel-Ziv complexity. *Neural Computation*, *16*(4), 717–736.

Arsiwalla, X. D., & Verschure, P. (2018). Measuring the Complexity of Consciousness. *Frontiers in Neuroscience*, *12*, 424.

Bayne, T., Hohwy, J., & Owen, A. M. (2016). Are There Levels of Consciousness? *Trends in Cognitive Sciences*, *20*(6), 405–413.

Becker, R., Van de Ville, D., & Kleinschmidt, A. (2018). Alpha Oscillations Reduce Temporal Long-Range Dependence in Spontaneous Human Brain Activity. *The Journal of Neuroscience: The Official Journal of the Society for Neuroscience*, *38*(3), 755–764.

Boncompte, G., Villena-González, M., Cosmelli, D., & López, V. (2016). Spontaneous Alpha Power Lateralization Predicts Detection Performance in an Un-Cued Signal Detection Task. *PloS One*, *11*(8), e0160347.

Bridi, M. C. D., Zong, F.-J., Min, X., Luo, N., Tran, T., Qiu, J., Severin, D., Zhang, X.-T., Wang, G., Zhu, Z.-J., He, K.-W., & Kirkwood, A. (2020). Daily Oscillation of the Excitation-Inhibition Balance in Visual Cortical Circuits. *Neuron*, *105*(4), 621–629.e4.

Brunel, N. (2000). Dynamics of networks of randomly connected excitatory and inhibitory spiking neurons. *Journal of Physiology, Paris*, *94*(5-6), 445–463.

494 Casali, A. G., Gosseries, O., Rosanova, M., Boly, M., Sarasso, S., Casali, K. R., Casarotto, S., Bruno,
495 M.-A., Laureys, S., Tononi, G., & Massimini, M. (2013). A theoretically based index of
496 consciousness independent of sensory processing and behavior. *Science Translational Medicine*,
497 *5*(198), 198ra105.
498 Chennu, S., O'Connor, S., Adapa, R., Menon, D. K., & Bekinschtein, T. A. (2016). Brain Connectivity
499 Dissociates Responsiveness from Drug Exposure during Propofol-Induced Transitions of
500 Consciousness. *PLoS Computational Biology*, *12*(1), e1004669.
501 D'Andola, M., Rebollo, B., Casali, A. G., Weinert, J. F., Pigorini, A., Villa, R., Massimini, M., &
502 Sanchez-Vives, M. V. (2018). Bistability, Causality, and Complexity in Cortical Networks: An In
503 Vitro Perturbational Study. *Cerebral Cortex* , *28*(7), 2233–2242.
504 Deco, G., Ponce-Alvarez, A., Hagmann, P., Romani, G. L., Mantini, D., & Corbetta, M. (2014). How
505 local excitation-inhibition ratio impacts the whole brain dynamics. *The Journal of Neuroscience:*
506 *The Official Journal of the Society for Neuroscience*, *34*(23), 7886–7898.
507 Dehghani, N., Peyrache, A., Telenczuk, B., Le Van Quyen, M., Halgren, E., Cash, S. S., Hatsopoulos,
508 N. G., & Destexhe, A. (2016). Dynamic Balance of Excitation and Inhibition in Human and
509 Monkey Neocortex. *Scientific Reports*, *6*, 23176.
510 Denève, S., & Machens, C. K. (2016). Efficient codes and balanced networks. *Nature Neuroscience*,
511 *19*(3), 375–382.
512 Destexhe, A., Rudolph, M., Fellous, J. M., & Sejnowski, T. J. (2001). Fluctuating synaptic
513 conductances recreate in vivo-like activity in neocortical neurons. *Neuroscience*, *107*(1), 13–24.
514 Destexhe, A., Rudolph, M., & Paré, D. (2003). The high-conductance state of neocortical neurons in
515 vivo. *Nature Reviews. Neuroscience*, *4*(9), 739–751.
516 Fazlali, Z., Ranjbar-Slamloo, Y., Adibi, M., & Arabzadeh, E. (2016). Correlation between Cortical State
517 and Locus Coeruleus Activity: Implications for Sensory Coding in Rat Barrel Cortex. *Frontiers in*
518 *Neural Circuits*, *10*, 14.
519 Ferenets, R., Lipping, T., Anier, A., Jäntti, V., Melto, S., & Hovilehto, S. (2006). Comparison of entropy
520 and complexity measures for the assessment of depth of sedation. *IEEE Transactions on Bio-*
521 *Medical Engineering*, *53*(6), 1067–1077.
522 Gao, R., Peterson, E. J., & Voytek, B. (2017). Inferring synaptic excitation/inhibition balance from field
523 potentials. In *NeuroImage* (Vol. 158, pp. 70–78).

https://doi.org/10.1016/j.neuroimage.2017.06.078

Gramfort, A., Luessi, M., Larson, E., Engemann, D. A., Strohmeier, D., Brodbeck, C., Parkkonen, L., & Hämäläinen, M. S. (2014). MNE software for processing MEG and EEG data. *NeuroImage*, *86*, 446–460.

Haider, B., Duque, A., Hasenstaub, A. R., & McCormick, D. A. (2006). Neocortical network activity in vivo is generated through a dynamic balance of excitation and inhibition. *The Journal of Neuroscience: The Official Journal of the Society for Neuroscience*, *26*(17), 4535–4545.

Haller, M., Donoghue, T., Peterson, E., Varma, P., Sebastian, P., Gao, R., Noto, T., Knight, R. T., Shestyuk, A., & Voytek, B. (n.d.). *Parameterizing neural power spectra*. https://doi.org/10.1101/299859

Harris, K. D., & Thiele, A. (2011). Cortical state and attention. *Nature Reviews. Neuroscience*, *12*(9), 509–523.

He, B. J. (2014). Scale-free brain activity: past, present, and future. *Trends in Cognitive Sciences*, *18*(9), 480–487.

He, B. J., & Raichle, M. E. (2009). The fMRI signal, slow cortical potential and consciousness. *Trends in Cognitive Sciences*, *13*(7), 302–309.

He, B. J., Zempel, J. M., Snyder, A. Z., & Raichle, M. E. (2010). The temporal structures and functional significance of scale-free brain activity. *Neuron*, *66*(3), 353–369.

Huupponen, E., Maksimow, A., Lapinlampi, P., Särkelä, M., Saastamoinen, A., Snapir, A., Scheinin, H., Scheinin, M., Meriläinen, P., Himanen, S.-L., & Jääskeläinen, S. (2008). Electroencephalogram spindle activity during dexmedetomidine sedation and physiological sleep. *Acta Anaesthesiologica Scandinavica*, *52*(2), 289–294.

Iemi, L., Chaumon, M., Crouzet, S. M., & Busch, N. A. (2017). Spontaneous Neural Oscillations Bias Perception by Modulating Baseline Excitability. *The Journal of Neuroscience: The Official Journal of the Society for Neuroscience*, *37*(4), 807–819.

Jas, M., Larson, E., Engemann, D. A., Leppäkangas, J., Taulu, S., Hämäläinen, M., & Gramfort, A. (2018). A Reproducible MEG/EEG Group Study With the MNE Software: Recommendations, Quality Assessments, and Good Practices. *Frontiers in Neuroscience*, *12*, 530.

Klimesch, W., Doppelmayr, M., Russegger, H., Pachinger, T., & Schwaiger, J. (1998). Induced alpha band power changes in the human EEG and attention. *Neuroscience Letters*, *244*(2), 73–76.

554 Lempel, A., & Ziv, J. (1976). On the Complexity of Finite Sequences. *IEEE Transactions on*
555 *Information Theory / Professional Technical Group on Information Theory*, *22*(1), 75–81.
556 Lombardi, F., Herrmann, H. J., & de Arcangelis, L. (2017). Balance of excitation and inhibition
557 determines 1/f power spectrum in neuronal networks. *Chaos* , *27*(4), 047402.
558 Manning, J. R., Jacobs, J., Fried, I., & Kahana, M. J. (2009). Broadband shifts in local field potential
559 power spectra are correlated with single-neuron spiking in humans. Journal of
560 Neuroscience, 29(43), 13613-13620.
561 Massimini, M., Ferrarelli, F., Huber, R., Esser, S. K., Singh, H., & Tononi, G. (2005). Breakdown of
562 cortical effective connectivity during sleep. *Science*, *309*(5744), 2228–2232.
563 Medel, V., Valdés, J., Castro, S., Ossandón, T., & Boncompte, G. (2019). Commentary: Amplification
564 and Suppression of Distinct Brainwide Activity Patterns by Catecholamines [Review of
565 *Commentary: Amplification and Suppression of Distinct Brainwide Activity Patterns by*
566 *Catecholamines*]. *Frontiers in Behavioral Neuroscience*, *13*, 217.
567 Miller, K. J., Honey, C. J., Hermes, D., Rao, R. P. N., denNijs, M., & Ojemann, J. G. (2014).
568 Broadband changes in the cortical surface potential track activation of functionally diverse
569 neuronal populations. *NeuroImage*, *85 Pt 2*, 711–720.
570 Miller, K. J., Sorensen, L. B., Ojemann, J. G., & den Nijs, M. (2009). Power-law scaling in the brain
571 surface electric potential. *PLoS Computational Biology*, *5*(12), e1000609.
572 Miskovic, V., MacDonald, K. J., Rhodes, L. J., & Cote, K. A. (2019). Changes in EEG multiscale
573 entropy and power-law frequency scaling during the human sleep cycle. *Human Brain Mapping*,
574 *40*(2), 538–551.
575 Nghiem, T.-A. E., Tort-Colet, N., Górski, T., Ferrari, U., Moghimyfiroozabad, S., Goldman, J. S.,
576 Teleńczuk, B., Capone, C., Bal, T., di Volo, M., & Destexhe, A. (2020). Cholinergic Switch
577 between Two Types of Slow Waves in Cerebral Cortex. *Cerebral Cortex* , *30*(6), 3451–3466.
578 Pfeffer, T., Avramiea, A.-E., Nolte, G., Engel, A. K., Linkenkaer-Hansen, K., & Donner, T. H. (2018).
579 Catecholamines alter the intrinsic variability of cortical population activity and perception. *PLoS*
580 *Biology*, *16*(2), e2003453.
581 Purdon, P. L., & Sampson, A. (2015). Clinical electroencephalography for anesthesiologistspart I:
582 background and basic signatures. *: The Journal of* ….
583 https://anesthesiology.pubs.asahq.org/Article.aspx?articleid=2430415

584 Reimer, J., Froudarakis, E., Cadwell, C. R., Yatsenko, D., Denfield, G. H., & Tolias, A. S. (2014). Pupil
585 fluctuations track fast switching of cortical states during quiet wakefulness. *Neuron*, *84*(2), 355–
586 362.
587 Rubenstein, J. L. R., & Merzenich, M. M. (2003). Model of autism: increased ratio of
588 excitation/inhibition in key neural systems. *Genes, Brain, and Behavior*, *2*(5), 255–267.
589 Rubin, R., Abbott, L. F., & Sompolinsky, H. (2017). Balanced excitation and inhibition are required for
590 high-capacity, noise-robust neuronal selectivity. *Proceedings of the National Academy of*
591 *Sciences of the United States of America*, *114*(44), E9366–E9375.
592 Sarasso, S., Rosanova, M., Casali, A. G., Casarotto, S., Fecchio, M., Boly, M., Gosseries, O., Tononi,
593 G., Laureys, S., & Massimini, M. (2014). Quantifying cortical EEG responses to TMS in (un)
594 consciousness. *Clinical EEG and Neuroscience: Official Journal of the EEG and Clinical*
595 *Neuroscience Society* , *45*(1), 40–49.
596 Schartner, M., Seth, A., Noirhomme, Q., Boly, M., Bruno, M.-A., Laureys, S., & Barrett, A. (2015).
597 Complexity of Multi-Dimensional Spontaneous EEG Decreases during Propofol Induced General
598 Anaesthesia. *PloS One*, *10*(8), e0133532.
599 Schaworonkow, N., & Voytek, B. (n.d.). Longitudinal changes in aperiodic and periodic activity in
600 electrophysiological recordings in the first seven months of life.
601 https://doi.org/10.1101/2020.08.18.256016
602 Sheehan, T. C., Sreekumar, V., Inati, S. K., & Zaghloul, K. A. (2018). Signal Complexity of Human
603 Intracranial EEG Tracks Successful Associative-Memory Formation across Individuals. *The*
604 *Journal of Neuroscience: The Official Journal of the Society for Neuroscience*, *38*(7), 1744–1755.
605 Sohal, V. S., & Rubenstein, J. L. R. (2019). Excitation-inhibition balance as a framework for
606 investigating mechanisms in neuropsychiatric disorders. In *Molecular Psychiatry* (Vol. 24, Issue 9,
607 pp. 1248–1257). https://doi.org/10.1038/s41380-019-0426-0
608 Tononi, G., & Edelman, G. M. (1998). Consciousness and complexity. *Science*, *282*(5395), 1846–
609 1851.
610 Trakoshis, S., Martínez-Cañada, P., Rocchi, F., Canella, C., You, W., Chakrabarti, B., Ruigrok, A. N.,
611 Bullmore, E. T., Suckling, J., Markicevic, M., Zerbi, V., MRC AIMS Consortium, Baron-Cohen, S.,
612 Gozzi, A., Lai, M.-C., Panzeri, S., & Lombardo, M. V. (2020). Intrinsic excitation-inhibition
613 imbalance affects medial prefrontal cortex differently in autistic men versus women. *eLife*, *9*.

https://doi.org/10.7554/eLife.55684

Uhlhaas, P. J., & Singer, W. (2010). Abnormal neural oscillations and synchrony in schizophrenia. *Nature Reviews. Neuroscience*, *11*(2), 100–113.

van Langen, J (2020). Open-visualizations for repeated measures in R. https://github.com/jorvlan/open-visualizations.

van Vreeswijk, C., & Sompolinsky, H. (1996). Chaos in neuronal networks with balanced excitatory and inhibitory activity. *Science*, *274*(5293), 1724–1726.

Virtanen, P., Gommers, R., Oliphant, T. E., Haberland, M., Reddy, T., Cournapeau, D., Burovski, E., Peterson, P., Weckesser, W., Bright, J., van der Walt, S. J., Brett, M., Wilson, J., Millman, K. J., Mayorov, N., Nelson, A. R. J., Jones, E., Kern, R., Larson, E., … SciPy 1.0 Contributors. (2020). SciPy 1.0: fundamental algorithms for scientific computing in Python. *Nature Methods*, *17*(3), 261–272.

Voytek, B., & Knight, R. T. (2015). Dynamic network communication as a unifying neural basis for cognition, development, aging, and disease. *Biological Psychiatry*, *77*(12), 1089–1097.

Waschke, L., Tune, S., & Obleser, J. (2019). Local cortical desynchronization and pupil-linked arousal differentially shape brain states for optimal sensory performance. *eLife*, *8*. https://doi.org/10.7554/eLife.51501

Welch, T. A. (1984). A technique for high-performance data compression. *Computer*, *6*, 8–19.

Wen, H., & Liu, Z. (2016). Broadband Electrophysiological Dynamics Contribute to Global Resting-State fMRI Signal. In *The Journal of Neuroscience* (Vol. 36, Issue 22, pp. 6030–6040). https://doi.org/10.1523/jneurosci.0187-16.2016

Wenzel, M., Han, S., Smith, E. H., Hoel, E., Greger, B., House, P. A., & Yuste, R. (2019). Reduced Repertoire of Cortical Microstates and Neuronal Ensembles in Medically Induced Loss of Consciousness. *Cell Systems*, *8*(5), 467–474.e4.

Yanagawa, T., Chao, Z. C., Hasegawa, N., & Fujii, N. (2013). Large-scale information flow in conscious and unconscious states: an ECoG study in monkeys. *PloS One*, *8*(11), e80845.

Zhang, X. S., Roy, R. J., & Jensen, E. W. (2001). EEG complexity as a measure of depth of anesthesia for patients. *IEEE Transactions on Bio-Medical Engineering*, *48*(12), 1424–1433.

Žiburkus, J., Cressman, J. R., & Schiff, S. J. (2013). Seizures as imbalanced up states: excitatory and inhibitory conductances during seizure-like events. *Journal of Neurophysiology*, *109*(5), 1296–

644 1306.

645

646 **Figures**
647

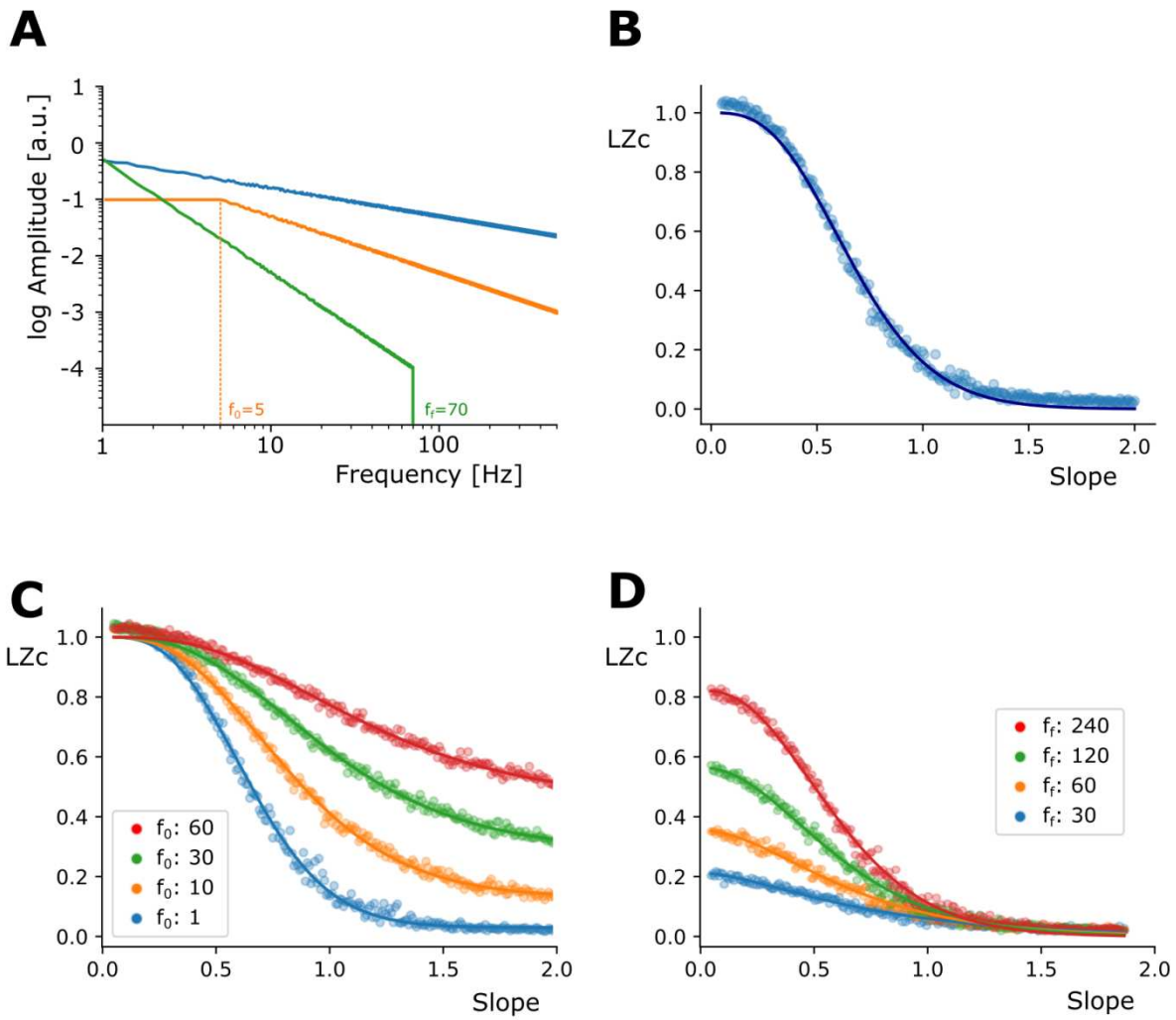

648
649
650 **Figure 1. iDFT models showcase the inverse relation between LZc and 1/f Slope. (A)** Illustration
651 of the amplitude spectrum in terms of frequency for signals composed using the iDFT model; f_0 and f_f
652 represent the initial and final frequency of the power law behavior. **(B)** Scatter plot of the LZc of 256
653 signals constructed with different 1/f slopes. Solid line corresponds to the best fit of Equation 3.1. **(C)**
654 and **(D)** illustrate the effect of including four different f_0's and f_f's in the construction of signals
655 respectively. Although the curves are scaled in comparison to (B), an homologous inverse relation is
656 observed.

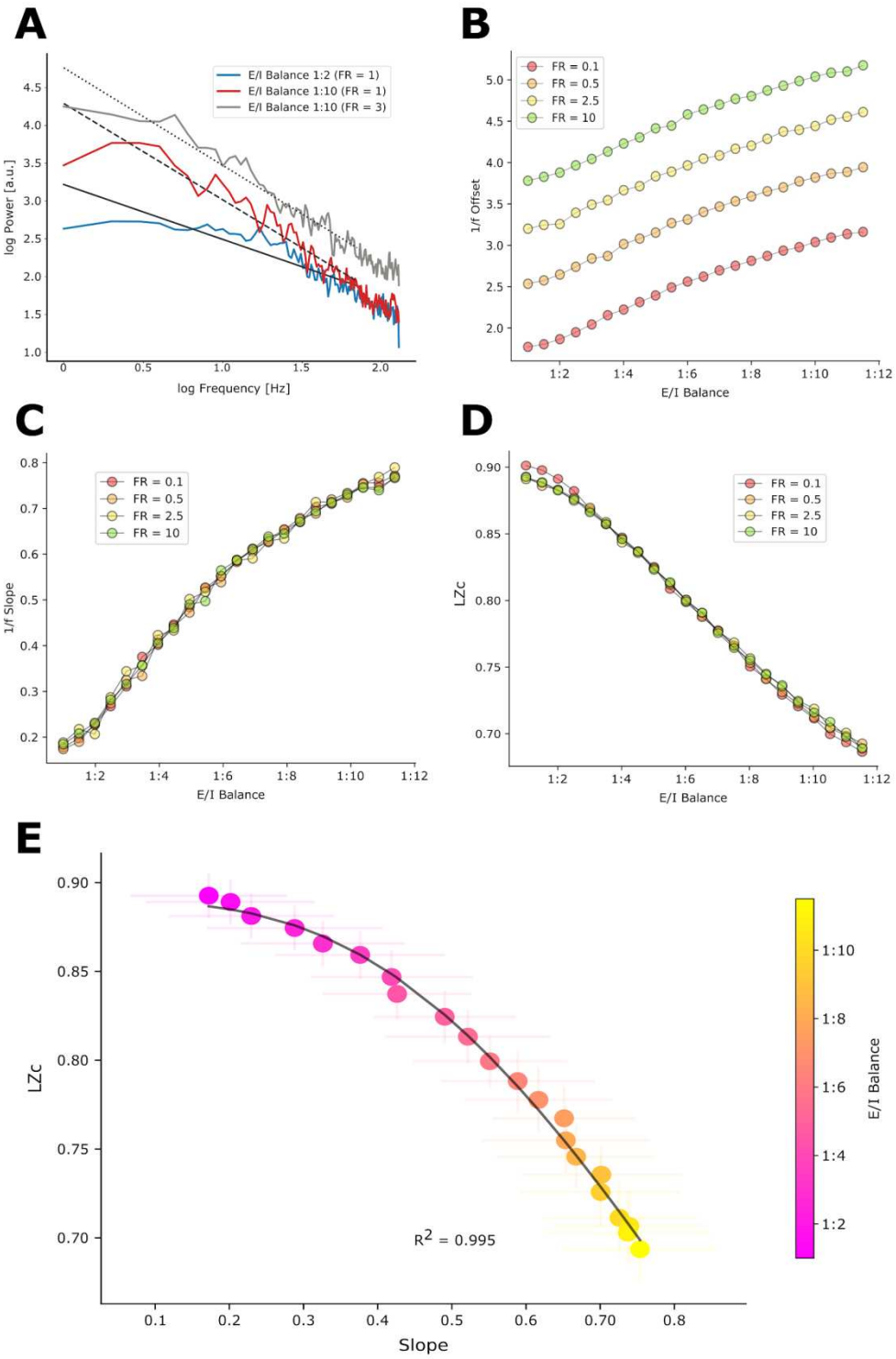

Figure 2. LZc and 1/f slope as a function of E/I balance. (A) Power Spectral Density plots of sample simulated brain signals with different E/I balances and total firing rates constructed using a cortical field potential model. **(B)** Plot showing the relation between offset and E/I balance, and its relation to firing rate. **(C)** Plots showing the positive relation between 1/f slope and E/I balance, which is independent of firing rate. **(D)** Plot showing the inverse relation between LZc and E/I balance. This relation was independent of firing rate. **(E)** Color scatter plot showcasing the relation observed between 1/f slope and LZc across a range of E/I balances (color bar) error bars represent the standard deviation across 100 simulations.

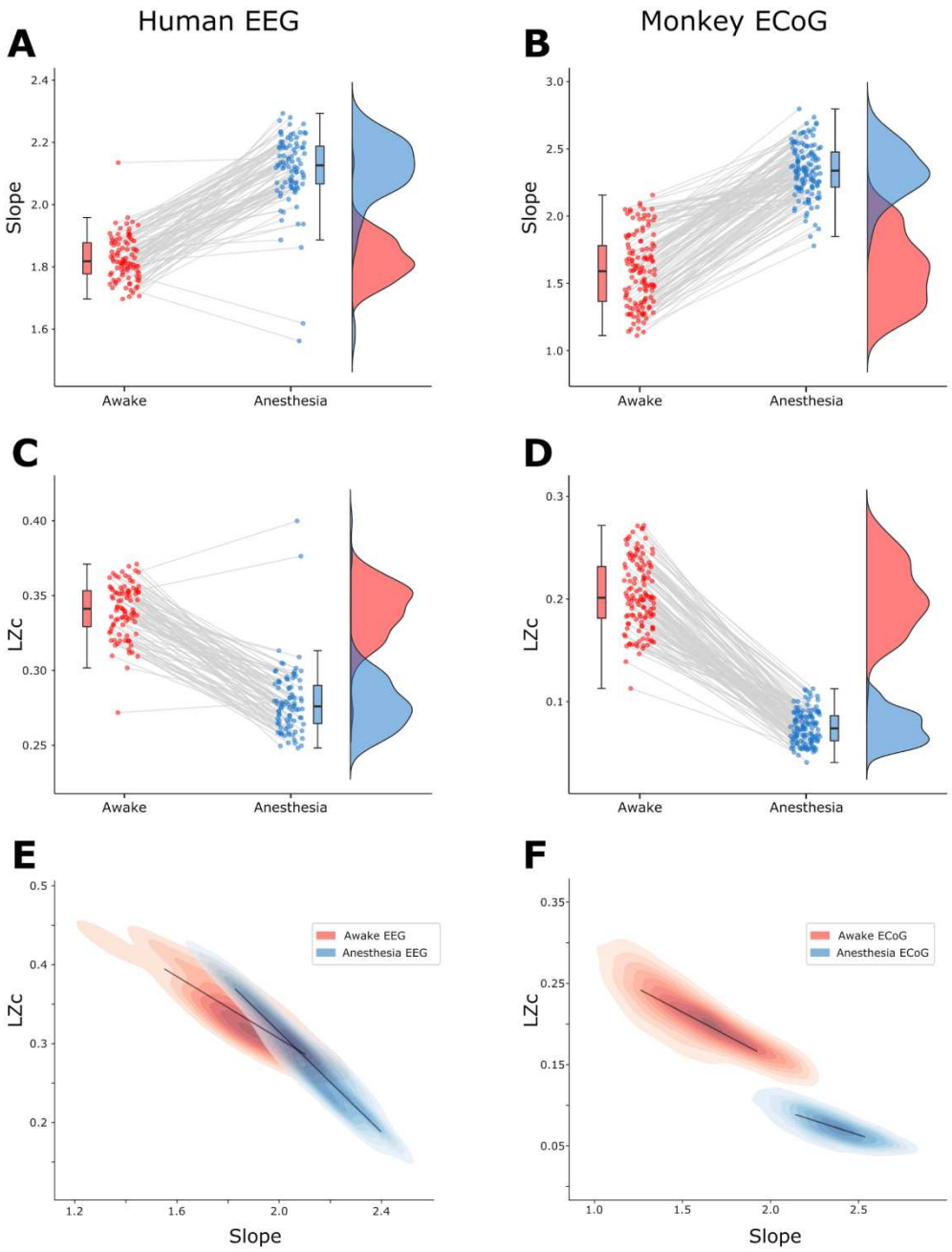

Figure 3. Propofol reduces LZc and steepens 1/f slope in human EEG and monkey ECoG data. **(A)** Propofol increases 1/f Slope across electrodes in human EEG data of a representative subject. In (A), (B), (C) and (D) each point depicts the average value (1/f slope or LZc) across time epochs for an electrode. Boxes depict the average value across electrodes, the range that includes 50% of points and the 2 standard deviations range. Density distributions across electrodes are plotted vertically on the right side of each plot. Blue and Red colors represent Awake and Anesthesia (propofol) respectively for all panels. **(B)** Average 1/f slope values for Awake and Anesthesia conditions for a representative monkey's ECoG data. **(C)** LZc in the same EEG dataset as (A) for Awake and Anesthesia conditions. **(D)** LZc in the same ECoG data as in (B) for Awake and Anesthesia. **(E)** Depicts a 2D density plot of the LZc vs 1/f slope of all epochs and electrodes for Awake and Anesthesia conditions. Black lines depict the average value, across electrodes, of the slope of the regressions performed between 1/f slope and LZc data (see methods). **(F)** Same as (E) but for ECoG data.